Astron. Astrophys. 353, 389–395 (2000)

ASTRONOMY AND ASTROPHYSICS

Small-scale topology of solar atmosphere dynamics

IV. On the relation of photospheric oscillations to meso-scale flows

Nick M. Hoekzema and Peter N. Brandt

Kiepenheuer-Institut für Sonnenphysik, Schöneckstrasse 6, 79104 Freiburg Br., Germany

Received 17 May 1999 / Accepted 14 October 1999

Abstract. We use a high quality five-hour sequence of images of the solar photosphere taken at the Swedish Solar Vacuum Telescope, La Palma, to study the relation of meso-scale divergence with the amplitudes of photospheric intensity oscillations. Meso-scale flows are determined by local correlation tracking of the granulation. Statistical evaluation of the co-location probability of regions with more than twice the average oscillation amplitude and regions with high or low meso-scale divergence shows that high amplitude regions are preferentially located in regions of negative divergence (convergence) and avoid meso-divergent regions. Additionally we confirm the increase of granule brightness in regions of positive divergence with the opposite effect in regions of convergence.

Key words: Sun: granulation – Sun: oscillations – Sun: photosphere

1. Introduction

There is evidence for at least three scales of motion in the solar photosphere: granulation, mesogranulation, and supergranulation. Granulation has been the subject of studies for more than a century, and its structure, physical properties and evolution are rather well known from both observational work and numerical models – except at the smallest spatial scales below 150 km on the Sun, which are unaccessible to present time ground-based and space-borne solar telescopes. Observed granular sizes range from the limit given by observational techniques, i.e. 150 km, to ≈ 2500 km (e.g., Roudier & Muller 1986; Hirzberger et al. 1997). Supergranulation had been detected by Leighton et al. (1962); gas rises at the supergranule's center, flows horizontally outwards at speeds of 200–500 m s^{-1}, and sinks at the cell boundary (cf. Simon 2000). Mean diameters quoted for supergranules range from 32 Mm (Simon & Leighton 1964) down to 13–18 Mm (Hagenaar et al. 1997), and seem to depend strongly on the material and method used for the determination.

The term mesogranulation was first used by November et al. (1981); they described the observed vertical motions as a "fairly stationary pattern of cellular flow with a spatial scale of 5–10 Mm", a spatial rms velocity amplitude of about 60 m s^{-1}, and a lifetime of "at least 2 hr". In the next decade some authors noted that granular structure seems to vary on meso-scales. Oda (1984) described repeatedly fragmenting granules that form a cellular pattern of 7 Mm size. Koutchmy & Lebecq (1986) artificially blurred a series of white light granulation images and found quasi-stationary intensity modulations at similar scales. Muller et al. (1990) noted that large granules seem to form a cellular pattern of a characteristic scale of 5 Mm. Later Brandt et al. (1991) found that size, intensity, lifetime, and expansion (collapse) rate of granules change with their location in the mesogranulation pattern.

Since its first detection nearly two decades ago, the properties of the mesogranulation were studied by various methods, especially by local correlation tracking (LCT, for a description see e.g. November 1986) and by two-dimensional spectroscopy (e.g. Straus & Bonaccini 1997). However, there is still disagreement on the nature of this phenomenon: whether it represents waves (Damé 1985; Straus & Bonaccini 1997) or convection (e.g. Deubner 1989; Straus et al. 1992); whether it is a distinct spatial regime (Title et al. 1986; Simon et al. 1988a; Ginet & Simon 1992) or cannot be identified as a regime separated from granulation (Straus et al. 1992; Straus & Bonaccini 1997). Accordingly, there is also wide disagreement on such basic properties as size and lifetime. While Simon et al. (1988b) quote sizes ranging from 3 to 9 Mm, with a mean around 6 Mm, Ueno & Kitai (1998a) find a mean size of as much as 13 Mm. In his thesis Darvann (1991) cites lifetimes to range from less than one half to many hours derived in work prior to 1991; his own measurements yield values between 3.5 and 7 hours, which is in good agreement with the values obtained by Brandt et al. (1994). In a recent paper Roudier et al. (1998) find much shorter lifetimes, i.e., ranging from 16 to 185 min depending on the temporal window and the methods used. The cited uncertainties demonstrate two basic difficulties concerning the meso-scale flows: i) the results are strongly method-dependent, especially they depend on where the limit between granulation and meso-granulation is defined; ii) long time series of very high spatial resolution are needed for a reliable determination of the meso-scale characteristics – a requirement that is very hard to fulfill by ground-based observations.

Send offprint requests to: P.N. Brandt (pnb@kis.uni-freiburg.de)

Concerning the topic of the relation between convection and oscillations, the search for the sources of solar oscillations has received considerable attention in recent years, as has the question how flow fields modulate the oscillations. Although Zaqarashvili (1999) suggests that 5-min waves are invoked by the radiative core of the Sun, most research concentrates on regions at, or just below, the solar surface because the velocity field here possesses the highest Mach number: the convective velocities are maximal and the velocity of sound is relatively low as compared to the interior.

Especially the impact of the granulation has been the topic of ongoing research. Rast (1995) argues that the turbulent downflows in intergranular lanes, in particular locations where the downflows gather into high velocity fingers, are strong emitters of acoustic energy. Indeed several observational studies (e.g., Rimmele et al. 1995; Goode & Strous 1998; Hoekzema et al. 1998b) confirm that acoustic waves in intergranular lanes on average have much higher amplitudes than in granules. However, this does not necessarily imply that intergranular spaces also are major sources of acoustic waves: the waves may be refracted or diffracted into them (Zhugzhda & Stix 1994; Hoekzema et al. 1998a). Simulations by Cattaneo et al. (1990) and Malagoli et al. (1990) suggest that the outflow near the edges of granules may reach the speed of sound thus invoking strong acoustic waves. This may have been observed indirectly by Nesis et al. (1992) and Solanki et al. (1996).

Much less attention has been given to relations between oscillations and larger-scale flow fields; but since there is no very great difference between the flow velocities associated with granulation, meso-scale flows, and supergranulation – all are of the order of 0.5 to several $\mathrm{km\,s^{-1}}$ – it is worthwhile to compare their impacts on acoustic wave amplitudes. Only recently Hoekzema & Brandt (1998) and Ueno & Kitai (1998b) analysed the impact of meso-scale flows on oscillations. Here we present results of a search for relations between intensity oscillation amplitudes and meso-scale flow patterns, i.e., meso-scale convergent regions and meso-scale divergent regions.

This paper builds on a series of papers: Hoekzema et al. (1998a, Paper I; 1998b, Paper II) and Hoekzema & Rutten (1998). They employ the correspondence factor C to explore local relations between fine structure and intensity oscillation amplitudes in the quiet solar photosphere on the basis of image sequences obtained with the Swedish Vacuum Solar Telescope (SVST) on La Palma. The approach here follows that of the preceding three papers. We use similar reduction and measurement procedures, and apply our Fourier analysis technique on brightness histories (per pixel) of almost 90 min duration to produce Fourier amplitude maps for spatial and temporal correlation with the concurrent photospheric meso-scale divergence maps. We measure the amount of spatio-temporal alignment at varying time delays between different features through the statistical correspondence factor C that was introduced in Paper I. It is used to quantify the co-spatiality of high oscillatory amplitudes with meso-scale morphology as measured by its divergence.

2. Data and analysis procedures

2.1. Observational data

The present analysis is based on a sequence of white light granulation images ($\lambda\,468 \pm 5\,\mathrm{nm}$) that was obtained on June 5, 1993 with the Swedish Vacuum Solar Telescope on La Palma (SVST, aperture 48 cm, see Scharmer et al. 1985 and Scharmer 1989). The observing and inititial reduction procedures have been described in detail by Simon et al. (1994). Frames were recorded by a Kodak Megaplus Model 1.4 CCD camera at a rate of 3.7 Hz. Each frame consisted of 1310 by 970 pixels with 8-bit digitization. A frame selection sytem (Scharmer & Lofdahl 1991) determined the rms contrast over a sub-field in real time. The two best images out of the 55 frames sampled per 15 s interval were recorded. The subsequent storage to magnetic tape took about 6 s; thus the total cycle time was about 21 s. For final analysis the better frame of each pair was selected. The image scale was 0.125 arcsec/pixel. Typical exposure times were 10–14 ms. The field of view was centered slightly south-east of the sunspot group NOAA 7519 which was situated at N05/E15 in the morning of June 5, 1993.

Thanks to excellent seeing conditions and the real-time frame selection, an image sequence of outstanding quality and length was obtained. From 8:07 to 19:07 UT the rms intensity contrast of most frames ranged between 6% and 10.6% with a median value of 8.1%. Fig. 1 of Paper II shows the temporal variation of the measured rms intensity contrast for the sequence. After corrections for dark current, flat field, rotation, transparency, and exposure variations the field of view was reduced to 460×434 pixels (41.7 Mm $\times$ 39.3 Mm); this field displayed quiet photosphere without magnetic activity. Mean photospheric intensity was normalized to 1.0. The frames were registered, corrected for instrumental profile, destretched to minimize seeing distortions, and interpolated to 21.05 s cadence, but not filtered subsonically, since this would spoil information on solar oscillations.

2.2. Fourier mapping

In order to reduce the frame-to-frame contrast changes caused by variable seeing, all granulation images were histogram equalized over 200 bins; i.e., the pixel brightnesses were rescaled such that there were equal numbers of pixels in each brightness bin. For example, the bin of brightness 1.00–1.01 contains 0.5% of the pixels, as does the maximum brightness bin 1.99–2.00.

The Fourier maps were constructed from three partly overlapping 89.5 min segments of 256 images each, centered at 12:45, 13:15, and 14:13 UT (see Fig. 3 for a schematic overview of the data sets); they represent a total of 513 images observed between 12:00 and 14:58 UT. The segments were apodized with a cosine bell to an effective duration of roughly 60 min to produce pixel-by-pixel Fourier amplitude maps for frequencies between 0 and 8.37 mHz (periods longer than 2 min) with a frequency resolution of 0.186 mHz. This duration is short enough to resolve meso-scale pattern evolution, while long enough to resolve wave modes with periods as long as 20 to 30 minutes.

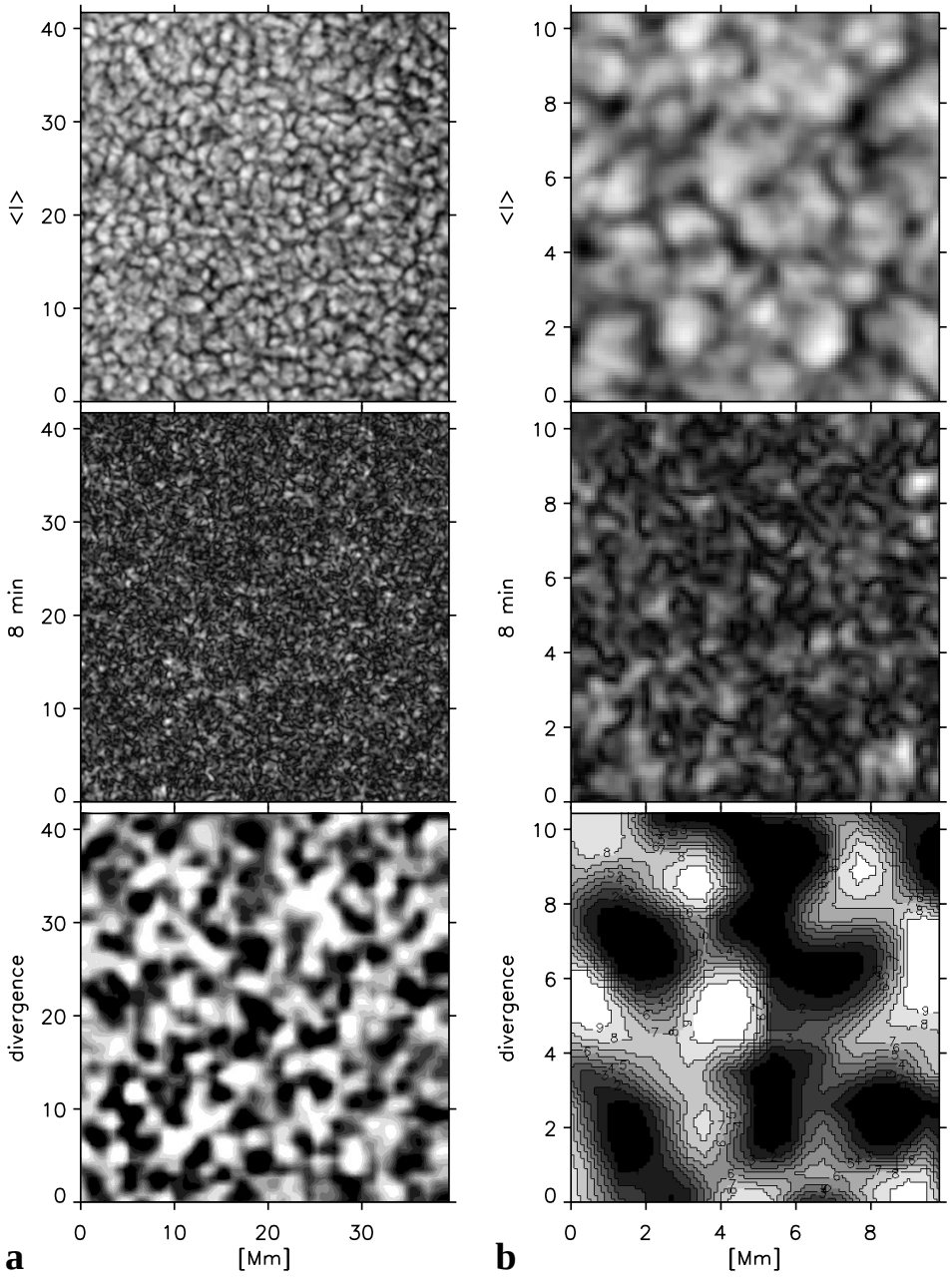

Fig. 1. **a**: granulation pattern averaged over 1 h (top); amplitude of the oscillation at periods around 8 minutes (middle); divergence of the granular proper motion determined by local correlation tracking (LCT) with positive divergence brighter than average (bottom). **b**: same quantities as in **a** shown for the lower left sub-field of each panel in **a**.

Since the three 89.5 min segments partly overlap, the results from the sequences are not completely independent. However, the overlap is not too large and the effect of overlap is further reduced by the apodizing which enhances the importance of images near the center of the segments and reduces it for images near the begin and end.

Fig. 1a (left column) shows an example of an 8 min amplitude map (middle panel) together with the intensity averaged over 1 h (top panel) as well as the divergence of the granular flow pattern (bottom panel). The right column, i.e., Fig. 1b, displays enlarged sections of each of the lower left sub-fields of Fig. 1a. A visual inspection of this figure puts forward the question which features in the amplitude map are co-spatial with positive or negative divergence. This is quantified by means of the correspondence factor C in Fig. 4. In the analysis below we make a distinction between amplitude maps of frequencies above 0.3 mHz and amplitude maps of lower frequency (i.e. the two lowest frequency channels) because the latter more or less display an intensity average of the granulation during the sequence. For frequencies above 0.3 mHz we investigate regions with amplitudes higher than twice the map average. They cover about 5% of the field.

For the lowest frequencies we took the maps at 0 mHz representing the average granulation and discarded those at 0.186 mHz because the latter were corrupted by the apodizing function that has precisely this frequency. The results of the co-location tests between *averaged granulation* and the divergence pattern are given in Fig. 4 at 0 mHz and at 0.186 mHz. However, in-

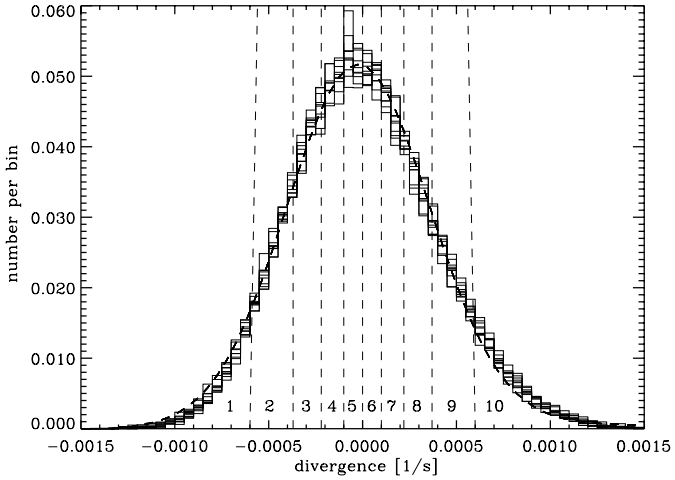

Fig. 2. Histograms of ten half-hour divergence maps, each of area 41.7 Mm $\times$ 39.3 Mm, plotted on top of each other; bin width is $5 \cdot 10^{-5}$ s^{-1}. For further analysis each divergence map was segmented into ten sub-maps 1... 10 each containing 10% of the number of pixels, as shown schematically.

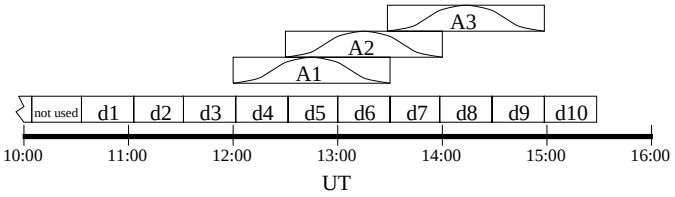

Fig. 3. Schematic presentation of the data sets used for analysis. The abscissa represents the time axis in UT of the observing day 5 June 1993. d1... d10 are 10 divergence maps of 29.8 min duration; the divergence maps were derived from averaging sets of 85 granule flow fields computed from neighbouring frames. A1... A3 are 3 sets of Fourier amplitude maps derived from partly overlapping 89.5 min sections of the image time series; time apodization is indicated by the bell shaped curves.

stead of working with pixels of twice the average amplitude (perhaps better called high brightness here), here we set the cut-off to larger than average and to larger than 1.10 the average. The former fill approximately 50% of the field, the latter about 45%. Note that we employ histogram-equalized images with a brightness distribution which is very different from the original images.

2.3. Divergence maps

Local correlation tracking with a 1.36 arcsec FWHM window was used to derive granular proper motion flow fields from pairs of images 21.05 sec apart. From sets of 86 frames thus 85 flow fields were computed covering a time span of $85 \cdot 21.05$ s, or 29.8 min each. After averaging sets of 85 flow fields a total of 10 averaged maps for the period 10:30 to 15:28 UT were obtained and the divergence of the averaged flows was computed; in most cases it ranged between $\pm 1.2 \cdot 10^{-3}$ s^{-1}. Fig. 2 shows the histograms of the divergence values of the 10 flow fields plotted on top of each other. The averaged distribution is rather smooth and very nearly symmetric, with a FWHM of $8.9 \cdot 10^{-4}$ s^{-1}. From each half-hour divergence map 10 segmented sub-maps were constructed, such that each sub-map contained 10% of the pixels, as shown schematically in Fig. 2. Thus sub-map 1 contains 10% of the pixels with strongest negative divergence, sub-map 2 the next 10%, and so on up to sub-map 10, which contains the 10% most positive divergence pixels. The 0.5 h average sub-maps were then submitted to a test for co-location with the corresponding Fourier amplitude maps as described in Sects. 2.4 and 2.5. The results for six of the sub-maps are presented in Fig. 4.

2.4. Correspondence factor

Spatial alignment is measured here with the correspondence factor C, a statistical tool which quantifies the cospatiality between two sub-sets of images or maps. This tool is comparable to the correlation factor but differs from it in that correlations must be calculated from full images, whereas correspondences may employ sub-fields. It was introduced in Sect. 3 of Paper I and is defined as $C = f_{AB}/f_B$, where $f_{AB} = N_{AB}/N_A$ is the fraction of pixels of type A in one map that also belong to type B in another map and $f_B = N_B/N$ is the filling factor of pixels of type B. C quantifies cospatiality as a random-draw likelihood. $C = 1$ suggests that A and B are independent phenomena while values $C > 1$ imply preferential co-location and $C < 1$ implies spatial avoidance. This statistical probability depends on spatial distribution only and may be estimated reliably from large data sets.

For example: the upper left panel of Fig. 1 displays the average of a sequence of 256 granulation images. Almost 50% of the pixels display a brightness above the average of the image. However, such pixels of high brightness constitute as much as 68% of the white regions in the lower left panel of Fig. 1 which represent the 10% of the field with the highest divergence. Therefore, the correspondence C between the regions with the highest divergence (sub-map 10 in Fig. 2) and pixels that are brighter than the field average is $0.68/0.50 = 1.36$. This tells us that if one chooses a pixel from the regions with highest divergence one has a 36% larger than random chance to pick one that is brighter than average.

2.5. Data structure and time delay charts

The temporal arrangement of the data sets and their use is demonstrated schematically in Fig. 3. As an example, the center line at Δt = 0 in the top panel of Fig. 4 is constructed from the computation of the correspondence between 3 simultaneous maps: sub-map 1 (10% strongest negative divergence pixels) of d5 vs. the amplitude maps of A1, sub-map 1 of d6 vs. A2, and sub-map 1 of d8 vs. A3. Values for Δt = 0.5 h represent C computed from sub-map 1 of d6 vs. A1, sub-map 1 of d7 vs. A2, and sub-map 1 of d9 vs. A3. Values for the other time lags in the top panel of Fig. 4 are computed accordingly – all for the 10% most negative divergence pixels of the 10 divergence maps. Each location in this frequency vs. time lag plot thus rep-

resents the mean of 3 correspondence values, except the lines at Δt = 1.5 h and 2.0 h for which A3 has no divergence maps taken 1.5 and 2 h later. From the variance of these averages one can estimate the σ and thus obtain a measure of the reliability. We find that the contour levels are spaced at roughly 1.5–2σ; in other words, the rms variations of C are about 0.05 to 0.07. It must be pointed out, however, that for $\Delta t \geq 1.5$ h the derived σ is not a very reliable estimate for the error, because it is derived from only 2 amplitude maps that are not fully independent.

The second panel from the top of Fig. 4 is created accordingly from the 10 divergence sub-maps 2, i.e., 10% of the pixels of divergence around $-5 \cdot 10^{-4}$ s^{-1} (see Fig. 2). The middle two panels of Fig. 4 represent C for very small divergence values just below and above zero, i.e. sub-maps 5 and 6, while the two bottom panels refer to the two most positive divergence bins (sub-maps 9 and 10). In the following we occasionally use the term "convergent" for regions of negative divergence.

3. Results

Fig. 4 displays time delay charts of the spatial correspondence C between pixels with Fourier amplitudes exceeding twice the average value and pixels of regions of strong negative divergence (i.e., sub-maps 1 and 2 of Fig. 2), of divergence near zero (i.e., sub-maps 5 and 6 of Fig. 2), or of high positive divergence (i.e., sub-maps 9 and 10 of Fig. 2). Each panel shows the spatial correspondence between the pixels of a given divergence submap and the pixels exhibiting over twice the average Fourier amplitude, as function of oscillation frequency (abscissa, corresponding periodicities along the top) and of time delay Δt; here $\Delta t > 0$ when maps of Fourier amplitudes are compared with *divergence maps taken later*. The correspondence values are displayed as greyscale contours in which values $0.9 < C < 1.1$ make up the background. Values of $C > 1.1$ are brighter than the background, those < 0.9 are darker. The contours are at 0.1 spacing; the contourline at $C = 1$ is omitted for clarity. The middle panels offer no significant relations, they display the results for the two sub-maps of near-zero divergence and show only a few isolated pixels, thus illustrating that the calculated σ is realistic.

The top panel of Fig. 4 refers to the 10% of the pixels with the highest negative divergence (sub-maps 1 of Fig. 2), i.e., strong convergence. Near $\Delta t = 0$ it shows high values for C (up to slightly more than 1.3) for almost all periods smaller than about 15 min. The effects set in at the moment that the divergence is observed (as far as we can tell from our limited time resolution of only 0.5 h) and then last 1–2 h for the 7–15 min oscillations and 1 h or less for shorter periods. The relations are less pronounced for periods shorter than 2.5 min and, markedly, also for the 5 min oscillations. The dark blob around $\Delta t = 0$ at the lowest frequencies tells us that there is more than a 20% *decrease of chance* ($C < 0.8$) as compared to random to find pixels that are brighter than average in strongly convergent regions; very probably this implies that they contain more (or larger) intergranular lanes. The dark blob for periods between 7 and 10 min at $\Delta t = 1$ h suggests that regions tend to have reduced oscillations of this periodicity roughly 1 h before convergence occurs in them. We suppose that all other specks in the panel are noise.

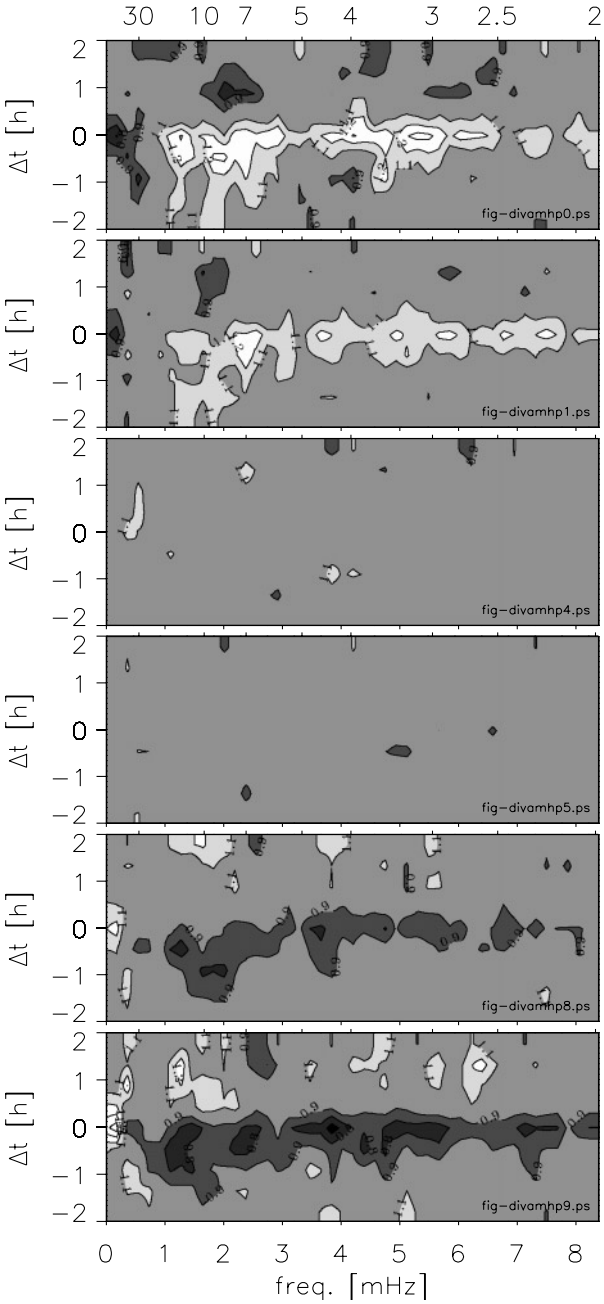

Fig. 4. Contour plot of the spatial correspondence C between high oscillatory amplitudes (exceeding twice the average) and sub-maps 1 . . . 10 of Fig. 2. Abscissa is oscillation frequency, ordinate is time lag. Values of $C > 1.1$ are brighter than the grey background, those < 0.9 are darker. Time lag is *positive* if amplitude maps are sampled *before* the divergence maps; temporal resolution is about 0.5 h. From top to bottom: sub-maps 1, 2, 5, 6, 9, 10 of Fig. 2.

The bottom panel of Fig. 4 is for the 10% of the pixels with the highest divergence, i.e., sub-maps 10 of Fig. 2. These pixels show very much the opposite patterning compared to the highly

negative divergence pixels: obviously large Fourier amplitudes tend to avoid regions with high divergence.

The panels in between are (from top to bottom) for sub-maps 2 (high convergence, but less then the highest 10%), for sub-maps 5 and 6 (divergence near zero) and for sub-map 9. They display a smooth transition between the extremes at top and bottom; the two middle panels are almost structureless and probably only display effects of noise. This is an indication that the effects are more or less symmetric, i.e., the excess of oscillation amplitudes in convergent regions is equally large as the deficit in the divergent regions. In this context we note that the correspondence factor C measures deviations from spatial averages, so that a blob of high correspondence in one panel must necessarily be compensated by a region of low correspondence at the same location in one or more of the other panels (including the ones that are not shown). The blankness of the middle panels implies that all effects seen in convergent regions are as strong as those in divergent regions but of opposite sign.

By a simple test we could corroborate that the results refer to the co-location of small-scale features. When we shift the divergence maps in steps spatially with respect to the amplitude maps, then the deviations from 1 of the correspondence factors computed from the shifted fields drop by a factor of order 3 for a shift of 1.2 arcsec, and they exhibit only noise for twice that shift. In other words, for a shift of larger than 2 arcsec the top and bottom panel of Fig. 4 would look like the two middle panels.

4. Discussion and conclusion

Fig. 4 proves that regions with Fourier amplitudes larger than twice the average show a strongly significant preference to coincide spatially with meso-scale convergent regions and to avoid meso-scale divergent regions. For amplitudes with periods in the range 2–15 min we find correspondences as large as 1.3 and as low as 0.7. Although the effects have up to 5–6σ significance they imply only small variations in oscillation amplitudes: pixels in sub-map 1 of the divergence maps, i.e., the strongest negative divergence (or strongly convergent) regions, display Fourier amplitudes of 3–3.5% above average, while those in sub-map 10, i.e. the strongest positive divergence regions, are 3–3.5% below average.

We attach some importance to the strong correspondence minimum of 0.7 (enhancement to 1.4) in the top (bottom) panel of Fig. 4 near frequency and $\Delta t \approx$ zero. This clearly hints at a *relation of average granule brightness to meso-scale structure*: brighter than average granules obviously prefer regions of strong positive divergence (bottom panel), while in strongly convergent regions (top panel) they are either darker on average or darker intergranular lanes prevail. This result confirms the earlier findings of Brandt et al. (1991), of increased granule brightness in regions of positive divergence, based on a different data set and a different analysis procedure.

In our opinion it is a puzzling feature of the correspondence maps for strong negative and positive divergence that oscillations of periods around 5 min show much less co-location probability than the other frequencies between 2.5 and 20 min. We cannot think of an explanation for this, the same holds for the features showing up in the top two and in the bottom maps of Fig. 4 around $\Delta t = 1$ h and periods of 8–10 min.

Our results for meso-scales are rather similar to those we found on a smaller scale for the normal granulation in Fig. 7 of Paper II. In that figure regions of more than twice the average Fourier amplitudes show much larger correspondences with intergranular lanes (which would be equivalent to meso-convergent regions here) than with granules (meso-divergent regions). While, as mentioned above, the strongest meso-convergent regions at periods below 3–4 min show an enhancement of amplitudes of 3–3.5% above average, in the darkest intergranular lanes the enhancement is about 4–4.5%. However, while there is no evidence that granulation modifies waves of periods longer than about 5 min, the meso-scale flows clearly are important for waves of periods as long as 10 to 15 min.

Whether the meso-scale flows mainly couple to oscillations by the direct influence of their spatial velocity and temperature modulation, or rather more indirectly by modifying the granular pattern is not obvious. On the one hand it is evident from Fig. 4, and the work of e.g., Brandt et al. (1991), that meso-scale flows and granulation are not independent phenomena: as compared to the average there are more granules (low oscillation amplitudes) in meso-scale divergent regions and more intergranular lanes (high oscillation amplitudes) in meso-scale convergent regions. Therefore, it seems highly probable that the variation of the granular pattern on meso-scales has at least some effect. The next article of this series will explore in more detail the relations between meso-scale flows and granulation, i.e., the preponderance of intergranular lanes in convergent and of granules in divergent regions – of which we see the signature in Fig. 4.

On the other hand Fig. 4 proves that there exists a clear relation of oscillations of periods longer than 5 min with meso-scale flows, but a similar relation with the granulation seems absent – at least our results in Papers I and II, and in Hoekzema & Rutten (1998) offer no hint for it. This is hard to understand if meso-scale flows were to have only an impact through modulation of the granular pattern. Also, it is easy to imagine meso-scale flows carrying along p-modes thus concentrating them in convergent regions and diluting them in divergent ones. The recent work on time-distance heloseismology (see for example Duvall et al. 1997) and on acoustic imaging of sub-surface layers (e.g., Chang et al. 1997) stresses the importance of flow fields for the propagation of acoustic waves; our results may well illustrate this.

Finally, we point out that the horizontal velocities of supergranular flows are about as large as those of the meso-scales and the granulation. Since granulation and meso-scale flows display comparable impact on oscillations, it would be interesting to analyse how supergranulation fits into the picture.

Acknowledgements. We thank G. Scharmer for the opportunity to observe at the SVST, G. Hosinsky, R. Kever, G. W. Simon, and W. Wang for observational support, as well as W. Mühlman and R. Shine for help in the pre-reduction of the data. M. Shand of DEC (Paris) supplied financial and technical assistance with the data acquisition system. The

SVST is operated on the island of La Palma by the Royal Swedish Academy of Sciences in the Spanish Observatorio del Roque de los Muchachos of the Instituto de Astrofísica de Canarias.

References

Brandt P.N., Ferguson S., Scharmer G.B., et al., 1991, A&A 241, 219
Brandt P.N., Rutten R.J., Shine R.A., Trujillo Bueno J., 1994, In: Rutten R.J., Schrijver C.J. (eds.) Solar Surface Magnetism. Kluwer Acad. Publ., 251
Cattaneo F., Hurlburt N., Toomre J., 1990, ApJ 349, L63
Chang H.-K., Chou D.-Y., LaBonte B., et al., 1997, Nat 389, L825
Damé L.E., 1985, In: Schmidt H.U. (ed.) Theoretical Problems in High Resolution Solar Physics. Max Planck Institut für Astrophysik, 244
Darvann T.A., 1991, Ph.D. Thesis, University of Oslo
Deubner F.-L., 1989, A&A 216, 259
Duvall Jr. T.L., Kosovichev A.G., Scherrer P.H., et al., 1997, Solar Phys. 170, 63
Ginet G.P., Simon G.W., 1992, ApJ 386, 359
Goode P.R., Strous L., 1998, In: Rimmele T., Balasubramaniam K.S., Radick R. (eds.) 19th NSO/SP Workshop on High Resolution Solar Physics: Theory, Observations, and Techniques
Hagenaar H.J., Schrijver C.J., Title A.M., 1997, ApJ 481, 988
Hirzberger J., Vazquez M., Bonet J.A., Hanslmeier A., Sobotka M., 1997, ApJ 480, 406
Hoekzema N.M., Brandt P.N., 1998, In: Rimmele T., Balasubramaniam K.S., Radick R. (eds.) 19th NSO/SP Workshop on High Resolution Solar Physics: Theory, Observations, and Techniques
Hoekzema N.M., Rutten R.J., 1998, A&A 329, 725
Hoekzema N.M., Rutten R.J., Brandt P.N., Shine R.A., 1998a, A&A 329, 276 (Paper I)
Hoekzema N.M., Brandt P.N., Rutten R.J., 1998b, A&A 333, 322 (Paper II)
Koutchmy S., Lebecq D., 1986, A&A 169, 323
Leighton R.B., Noyes R.W., Simon G.W., 1962, ApJ 135, 474
Malagoli A., Cattaneo F., Brummell N.H., 1990, ApJ 361, L33
Muller R., Roudier Th., Vigneau J., 1990, Solar Phys. 126, 53
Nesis A., Bogdan T.J., Cattaneo F., et al., 1992, ApJ 399, L99
November L.J., 1986, Appl. Opt. 25, 392
November L.J., Toomre J., Gebbie K.B., Simon G.W., 1981, ApJ 245, L123
Oda N., 1984, Solar Phys. 93, 243
Rast M.P., 1995, ApJ 443, 863
Rimmele T.R., Goode P.R., Harold E., Stebbins R.T., 1995, ApJ 444, L119
Roudier Th., Muller R., 1986, Solar Pys. 107, 11
Roudier Th., Malherbe J.M., Vigneau J., Pfeiffer B., 1998, A&A 330, 1136
Scharmer G.B., 1989, In: Rutten R.J., Severino G. (eds.) Solar and Stellar Granulation. Kluwer Ac. Publ., 161
Scharmer G.B., Lofdahl M., 1991, Adv. Space Res. 11, 129
Scharmer G.B., Petterson L., Brown D.S., Rehn J., 1985, Appl. Opt. 24, 2558
Simon G.W., 2000, In: Encyclopedia of Astronomy and Astrophysics. Inst. of Phys. Publ., Bristol/Macmillan, London, to be published
Simon G.W., Leighton R.B., 1964, ApJ 140, 1120
Simon G.W., Title A.M., Topka K.P., et al., 1988a, ApJ 327, 964
Simon G.W., November L.J., Acton L.W., et al., 1988b, Adv. Space Res. 8, (7)169
Simon G.W., Brandt P.N., November L.J., Scharmer G.B., Shine R.B., 1994, In: Rutten R.J., Schrijver C.J. (eds.) Solar Surface Magnetism. Kluwer Ac. Publ., 261
Solanki S.K., Rüedi I., Bianda M., Steffen M., 1996, A&A 308, 623
Straus Th., Bonaccini D., 1997, A&A 324, 704
Straus Th., Deubner F.-L., Fleck B., 1992, A&A 256, 652
Title A.M., Tarbell T.D., Simon G.W., the SOUP Team, 1986, Adv. Space Res. 6, 253
Ueno S., Kitai R., 1998a, PASJ 50, 125
Ueno S., Kitai R., 1998b, In: Deubner F.-L., Christensen-Dalsgaard J., Kurtz D. (eds.) New Eyes to see inside the Sun and Stars. IAU Symp. No. 185, 457
Zaqarashvili T., 1999, A&A 341, 617
Zhugzhda, Y.D., Stix M., 1994, A&A 291, 310